Intensity dependence of the attosecond control of the dissociative ionization of D_2

H Li[1,2]**, A S Alnaser**[1,3,4]**, X M Tong**[5,6]**, K J Betsch**[1]**, M Kübel**[1,2]**,
T Pischke**[1]**, B Förg**[1,2]**, J Schötz**[1,2]**, F Süßmann**[1,2]**, S Zherebtsov**[1]**,
B Bergues**[1]**, A Kessel**[1]**, S A Trushin**[1]**, A M Azzeer**[4]** and M F Kling**[1,2]

[1] Max-Planck-Institut für Quantenoptik, D-85748 Garching, Germany

[2] Department of Physics, Ludwig-Maximilians-Universität München, D-85748 Garching, Germany

[3] Physics Department, American University of Sharjah, PO Box 26666, Sharjah, UAE

[4] Physics and Astronomy Department, King Saud University, Riyadh 11451, Saudi Arabia

[5] Institute of Materials Science, University of Tsukuba, Ibaraki 305-8573, Japan

[6] Center for Computational Sciences, University of Tsukuba, Ibaraki 305-8577, Japan

E-mail: matthias.kling@lmu.de

Abstract

Light-field driven electron localization in deuterium molecules in intense near single-cycle laser fields is studied as a function of the laser intensity. The emission of D^+ ions from the dissociative ionization of D_2 is interrogated with single-shot carrier–envelope phase (CEP)-tagged velocity map imaging. We explore the reaction for an intensity range of $(1.0–2.8) \times 10^{14}$ W cm^{-2}, where laser-driven electron recollision leads to the population of excited states of D_2^+. Within this range we find the onset of dissociation from 3σ states of D_2^+ by comparing the experimental data to quantum dynamical simulations including the first eight states of D_2^+. We find that dissociation from the 3σ states yields D^+ ions with kinetic energies above 8 eV. Electron localization in the dissociating molecule is identified through an asymmetry in the emission of D^+ ions with respect to the laser polarization axis. The observed CEP-dependent asymmetry indicates two mechanisms for the population of 3σ states: (1) excitation by electron recollision to the lower excited states, followed by laser-field excitation to the 3σ states, dominating at low intensities, and (2) direct excitation to the 3σ states by electron recollision, playing a role at higher intensities.

Keywords: carrier–envelope phase, strong-field physics, electron dynamics, molecular dynamics

(Some figures may appear in colour only in the online journal)

1. Introduction

Intense, laser pulses with well-defined waveforms have been used to control and investigate sub-femtosecond electron dynamics in atoms [1, 2], molecules [3], nano-systems [4, 5] and solids [6–8]. The control over the electric field of light pulses permits the force acting on electrons on attosecond timescales to be controlled [9]. An approach to interrogate field-driven dynamics is to alter the carrier–envelope phase (CEP) of few-cycle laser pulses interacting with the target. The electric field of light pulses, e.g. given as $E(t) = E_0(t)$ cos $(\omega t + \phi)$, depends on the envelope function $E_0(t)$, the angular frequency ω and the CEP ϕ, where for decreasing pulse duration the CEP plays an increasing role in the pulse waveform. The recent development of CEP-tagging [10–12], where instead of stabilizing the CEP [13], its value is measured for every single laser shot together with the data from the laser–target interaction, has given rise to a significant improvement in the signal-to-noise ratio of related experiments [14–16]. Here, we employ the technique in studies on the intensity dependence of the dissociative ionization of D_2 molecules in near-single cycle laser fields.

The hydrogen molecule and its isotopes are model systems in strong-field molecular physics and related studies

have been a key in improving our understanding of the interaction of strong fields with molecular targets. Since the first experimental work on controlling electron localization in the dissociative ionization of D_2 in intense few-cycle laser fields [17], further studies have been carried out on molecular hydrogen and its isotopes using CEP-stabilized few-cycle near-infrared [18–21] and mid-infrared pulses [22]. Sub-cycle control has also been achieved and investigated with two-colour synthesized femtosecond pulses [23, 24], angular streaking with circular polarized pulses [25] and with a combination of attosecond extreme ultraviolet and near-infrared pulses [26, 27]. With the advent of the CEP-tagging technique, experiments have become possible on hydrogen molecular ion beam targets [28, 29]. These previous experimental studies on electron localization in molecular hydrogen addressed the principal control mechanisms, reaction pathways, and the wavelength and pulse duration dependence of the control [3]. However, despite this significant progress and theoretical predictions [30, 31], the intensity dependence of the electron localization has not been explicitly studied experimentally. Here, we study the intensity dependence of the dissociative ionization of D_2 molecules and CEP-control of electron localization in the reaction. Using near-single cycle laser pulses allows us to investigate a larger intensity range as compared to the situation with longer pulses [32], where significant double ionization occurs that hampers the observation of the directional ion emission.

Many theoretical studies have addressed the mechanisms of the sub-cycle control of electron localization (see e.g. [30, 31, 33–38]). While the strong-field interaction with the hydrogen molecular ion can be treated exactly with quantum mechanical computations (see e.g. [29, 33, 34, 39]), this has been difficult for the interaction of strong fields with neutral hydrogen molecules [36]. The development of suitable theoretical models that accurately describe the interaction of strong fields with neutral hydrogen molecules and predict experimental results is thus very desirable. The development of such models largely benefits from multi-dimensional experimental data that provide rigid constraints for testing the models.

The interaction of the neutral hydrogen molecule with a strong laser field typically results in the generation of the cation through an initial ionization by the laser field. Previous experimental and theoretical studies have established that electron localization in the dissociating hydrogen molecular ion, which can be detected by the directional ion emission upon its fragmentation, is induced by the coupling of odd and even states by the laser field(s) [3]. The molecular cation may also be formed from highly excited states of the neutral molecule, which are populated by the laser and autoionize [27, 40]. The latter process has been studied in detail theoretically by Martin and coworkers [27, 40–43] and has been invoked as a possible explanation for the directional emission of fragment ions in the dissociative ionization of molecular hydrogen in a pump-probe experiment with attosecond extreme ultraviolet and few-cycle near-infrared pulses [27].

The pathways which result in the population of excited states of the hydrogen molecular ion can be controlled by the

laser pulse duration and intensity [44]. Many of the earlier studies have focused on the low fragment ion kinetic energy channels that correspond to dissociation by bond softening (BS) [45] or through above-threshold dissociation (ATD) [21]. High-energy fragment ions can be created through population of higher lying excited states of the cation. One route for the population of the 2σ state of H_2^+ and its isotopes and also of higher lying states is the recollisional excitation (RCE) of the ground state molecular ion with the laser-driven electron from the initial ionization. Directional atomic ion (H^+/D^+) emission at kinetic energies in the range 3–8 eV was assigned to this dissociation pathway [17]. Although higher kinetic energies for atomic ions from the dissociative ionization of molecular hydrogen and its isotopes have been observed [17, 19, 22, 46], the directional control of the ion emission at such energies has not been reported.

Here, we use near-single cycle laser pulses of 4 fs duration at 730 nm to study the dependence of the electron localization in the dissociative ionization of D_2 on the CEP and laser intensity. We report on the observation of the directional ion emission for D^+ kinetic energies above 8 eV. Quantum mechanical simulations show that dissociation from the 3σ states of D_2^+ is responsible for the observed CEP and laser-intensity dependence.

2. Experimental approach

The experimental apparatus was discussed in detail in [47]. Briefly, few-cycle pulses are generated by sending a beam of 25 fs near-infrared pulses (centred at 790 nm) at a repetition rate of 1 kHz through a hollow core fibre (HCF) and chirped mirror compressor. The HCF is filled with 2 bar of Ne gas. The compressor delivers 4 fs pulses centred at 730 nm that are split by an 80/20 broadband beam splitter. The main part is sent to a single-shot velocity map imaging (VMI) spectrometer and the small portion to a single-shot stereo-ATI phasemeter [12]. Wedge pairs are installed in both beam paths for dispersion compensation.

The linearly polarized 4 fs laser beam is focused onto an effusive gas jet in the VMI chamber by a mirror with $f = 25$ cm. The laser polarization is vertical (along the y-direction) and parallel to the VMI detector plane (x–y). A continuous variable neutral density filter served to adjust the laser intensity. Electrons and ions from the laser–target interaction are projected by the VMI electrodes along the z-axis to the two-dimensional detector assembly consisting of micro-channel plates (MCPs) and a phosphor screen (Hamamatsu F2226–24P136). The light flashes on the phosphor screen are recorded at a kHz rate with a complementary metal-oxide semiconductor (CMOS) camera (GSVitec).

Typical D_2 gas pressures used in the chamber are of the order of 10^{-7} to 10^{-6} mbar with a background pressure of about 5×10^{-9} mbar. The target gas pressure is adjusted for different laser intensities to obtain moderate signal counts for each laser shot and avoid space charge effects. The voltage on the MCPs is gated by a high-voltage switch to record D^+ ions. For each laser pulse that is sent to the VMI, the CEP can be obtained from the corresponding data point on the parametric

asymmetry plot (PAP) [48] detected by the phasemeter. In the data analysis, the obtained PAP is divided into 20 equal angle ranges. The corresponding VMI images within the same angle bin are summed up, resulting in 20 images for the CEP range from 0 to 2π. Higher CEP resolution can be obtained by choosing a larger number of bins. Note that the CEPs obtained here are relative phases; there is a constant phase shift between the pulses that are measured by the phasemeter and those in the VMI spectrometer. The resulting VMI images are Abel inverted [49], permitting slices to be extracted through the 3D momentum distributions (here we show slices at $z = 0$). Laser intensities in the experiments are varied with a neutral density filter and estimated by measuring the cutoff energy of rescattered electrons from Xe under identical laser conditions.

3. Theoretical modelling

3.1. Model for the quantum mechanical simulations

In our simulations we assume a two-step process for the creation of D^+ ions in the intense laser field: (1) the formation of ground state D_2^+ from D_2 by tunnelling ionization, occurring at time t_0, and (2) the dissociation of D_2^+ in the remainder of the laser field either directly from the ground state of D_2^+ or dissociation of D_2^+ from excited electronic states that are produced through recollision excitation when the ejected electron returns to the parent core at time t_r. The returning time t_r and the returning energy E_r of the electron are obtained by a semi-classical simulation [50]. Then the time evolution of the D_2^+ nuclear wave packet in the laser field can be obtained by solving the following coupled channel time-dependent Schrödinger equation (TDSE),

$$i\frac{\partial}{\partial t}\Psi_{i,s}(R,t) = H_{i,s}(R)\Psi_{i,s}(R,t) + \sum_{j,s'} V_{i,s}^{j,s'}(R,t)\Psi_{j,s'}(R,t).$$
(1)

Here the index i or j stands for $1\sigma, 2\sigma, 3\sigma$ and π states and s (s') stands for the gerade or ungerade states, $H_{i,s}(R) = -\nabla^2/2 + U_{i,s}(R)$ is the Hamiltonian associated with a given potential curve $U_{i,s}(R)$, and $V_{i,s}^{j,s'}(R,t)$ is the interaction between the i, s and j, s' states coupled by the laser field.

For a given initial state created at time t_r, we propagate the NWP (nuclear wave packets) in the IR field by equation (1). When the IR field is over, the NWP can be expressed as

$$\Psi(R) = \sum_i \int [C_{i,g}(E)\chi_{i,g}(R,E) + C_{i,u}(E)\chi_{i,u}(R,E)]\,dE,$$
(2)

which depends on the initial condition, laser parameters and the angle between the IR field and molecular axis. Here $\chi_{i,g}(R,E)$ is the energy normalized continuum nuclear wavefunction for a given dissociative energy E, and $C_{i,g}$ is the amplitude.

We have not accounted for an energy shift due to the screening effect from the ionized electrons [51]. If we assume that the screening parameter (the Debye length) is $\lambda_d = 20 + 5*R^2$, the kinetic energy of D^+ ions can shift by about 1 eV. Deviations between the theoretical and experimental kinetic energy spectra may originate from such screening effects.
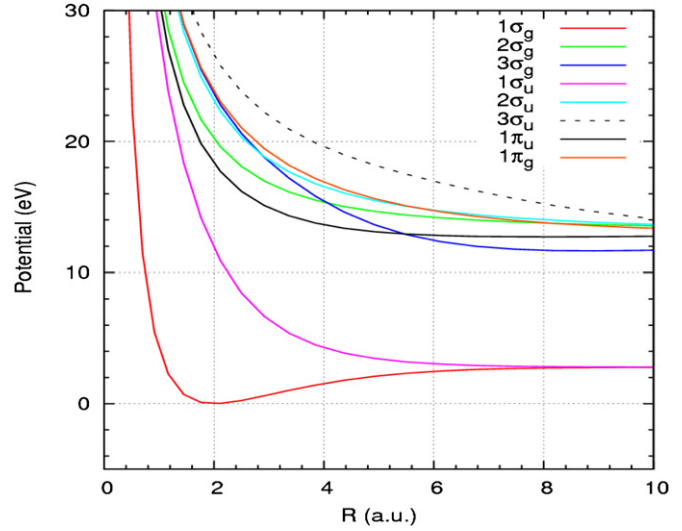

Figure 1. The first eight potential energy curves of D_2^+ used in the simulation. The curves were calculated in prolate spheroidal coordinates as detailed in [52].

For linearly polarized ultrashort pulses with the polarization in vertical (up–down) direction, the electron localization to the up or down direction with the dissociation energy E is

$$C_{\text{up}}(E,t_0) = \frac{1}{2}\sum_i |C_{i,g}(E)\exp[i\delta_{i,g}(E)]$$
$$+ C_{i,u}(E)\exp[i\delta_{i,u}(E)]|$$
(3)

and

$$C_{\text{down}}(E,t_0) = \frac{1}{2}\sum_i |C_{i,g}(E)\exp[i\delta_{i,g}(E)]$$
$$- C_{i,u}(E)\exp[i\delta_{i,u}(E)]|,$$
(4)

where $\delta_{i,g}(E)$ and $\delta_{i,u}(E)$ are the phase shifts for the gerade and ungerade states at a given dissociation energy E. The first eight potential curves of D_2^+, which lead to dissociation to $D(n = 1,2)$ states, where n is the principle quantum number of hydrogen atoms, are shown in figure 1.

3.2. Direct IR field dissociation

If we assume that the deuterium molecule is ionized by the laser field at time t_0, then the initial condition for equation (1) is $\Psi_{1\sigma_g}(R,t_0) = \sqrt{W(R,t_0)}\chi_g(R)$, where $W(R,t_0)$ is the molecular tunnelling ionization rate [53] at a given nuclear separation R and time t_0 with the over-barrier correction [54] and $\chi_g(R)$ is the vibrational ground state wavefunction of D_2, assuming that the Franck–Condon principle is applicable in the tunnelling ionization process. The dissociation probability is calculated from equation (1) with the given initial condition for each time t_0, then the dissociation of the D^+ ion to the up/down direction is expressed as

$$P_{\text{up/down}}^{\text{dis}}(E) = \int |C_{\text{down/up}}(E,t_0)|^2 dt_0.$$
(5)

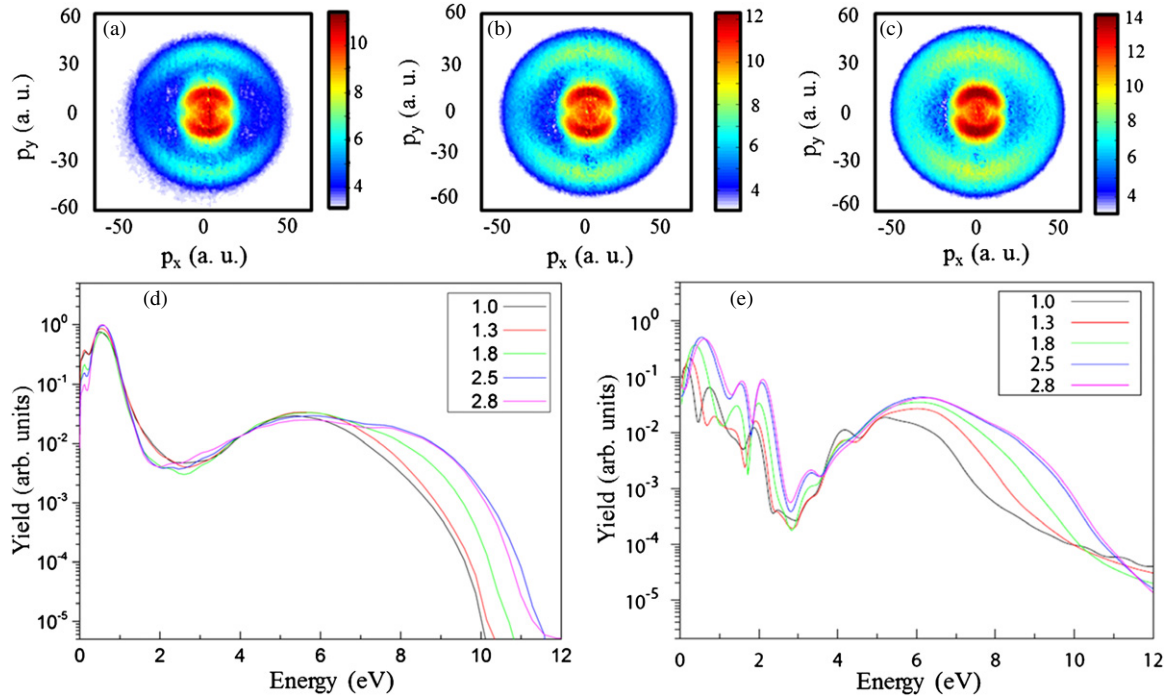Note that the D^+ goes to the opposite direction of the localized electron.

Figure 2. (a)–(c) CEP averaged inverted VMI images for D^+ ions in a 4 fs laser field at intensities of $(1.0 \pm 0.3) \times 10^{14}$ W cm^{-2}, $(1.8 \pm 0.3) \times 10^{14}$ W cm^{-2} and $(2.5 \pm 0.3) \times 10^{14}$ W cm^{-2}, respectively. (d), (e) Energy spectra for D^+ ions from D_2 obtained for the laser intensities indicated in the legend (in units of 10^{14} W cm^{-2}) for experiments and simulations, respectively. For better visibility of the high-energy tail, the spectra have been normalized to their values at 4 eV.

3.3. Recollision-induced dissociation

For recollision-induced dissociation, we assume that the D_2 is ionized by the laser field at time t_0 and the electron returns to the parent core after time t_r, then the initial condition for equation (1) is $\Psi_{j,s}(R, t_0 + t_r) = \sqrt{P_{j,s}(R, t_r)} \exp(-iH_{1\sigma_g} t_r) \sqrt{W(R, t_0)} \chi_g(R)$, where $P_{j,s}(R, t_r)$ stands for the electron impact excitation probability to the j, s states at R position and $H_{1\sigma_g}$ is the vibrational Hamiltonian associated with the D_2^+ ground electronic state. Similar to the IR field dissociation, the dissociation of D^+ to the up/down direction is expressed as

$$P_{\text{up/down}}^{\text{res}}(E) = \int |C_{\text{down/up}}(E, t_0, t_r)|^2 \, dt_0 \, dt_r. \qquad (6)$$

The D^+ ions emitted to the up or down directions depend on CEP and their kinetic energy. The asymmetry parameter A_{th}, indicating the directionality of the emission, is then defined as

$$A_{\text{th}}(\phi, E) = \frac{P_{\text{up}}(\phi, E) - P_{\text{down}}(\phi, E)}{P_{\text{up}}(\phi, E) + P_{\text{down}}(\phi, E)}. \qquad (7)$$

4. Results and discussion

4.1. Momentum maps and kinetic energy spectra of D^+ ions for different intensities

Momentum maps and kinetic energy spectra of D^+ ions obtained from the experiments for different laser intensities are shown in figure 2. The momentum maps may contain small contaminations of H_2^+ ions from the ionization of background H_2 (which appears as a dot in the centre of

the momentum maps). Contributions below 0.2 eV are thus neglected in our discussion. The strong peak around 0.7 eV (see figure 2(d)) arises from dissociation of the D_2^+ ground state via BS. The contributions with radial momenta $p_r = (p_x^2 + p_y^2)^{1/2}$ around 12 au correspond to this region. The higher energy contributions above 3 eV (with p_r above 25 au) arise from dissociation of excited states of D_2^+ that are populated by either the laser field or recollision with the electron from the ionization of the neutral molecule (RCE) or both. As inferred from the very broad angular distribution, for the intensity range used in our study, (1.0–2.8) $\times$ 10^{14} W cm^{-2}, and near-single cycle pulses, the population of the excited states by a process involving electron recollision is dominating.

A contribution at around 2–3 eV is increasing above 2.5 $\times$ 10^{14} W cm^{-2} (see figure 2(d)) and filling the gap between the peaks for BS and RCE, which we assign to a combination of ATD [21] and enhanced ionization [55]. The main change in the spectra that we focus on in the present study is the observation of D^+ kinetic energies above 8 eV. As the intensity increases from 1.0 to 2.8 $\times$ 10^{14} W cm^{-2}, the recollision peak becomes broader and extends into a higher energy region. This contribution has been observed as a weak signal in studies on D_2 with few-cycle pulses at 760 nm [17] and at 2.1 μm [22]. Its intensity dependence and the directional emission of D^+ ions in this region, which are analysed below, have, however, not been reported. Figure 2(e) shows D^+ spectra obtained from the simulations. As we elaborate below, the simulations indicate that the contribution above 8 eV originates from the dissociation of higher-lying excited states of D_2^+. Note that the current simulations do not contain contributions
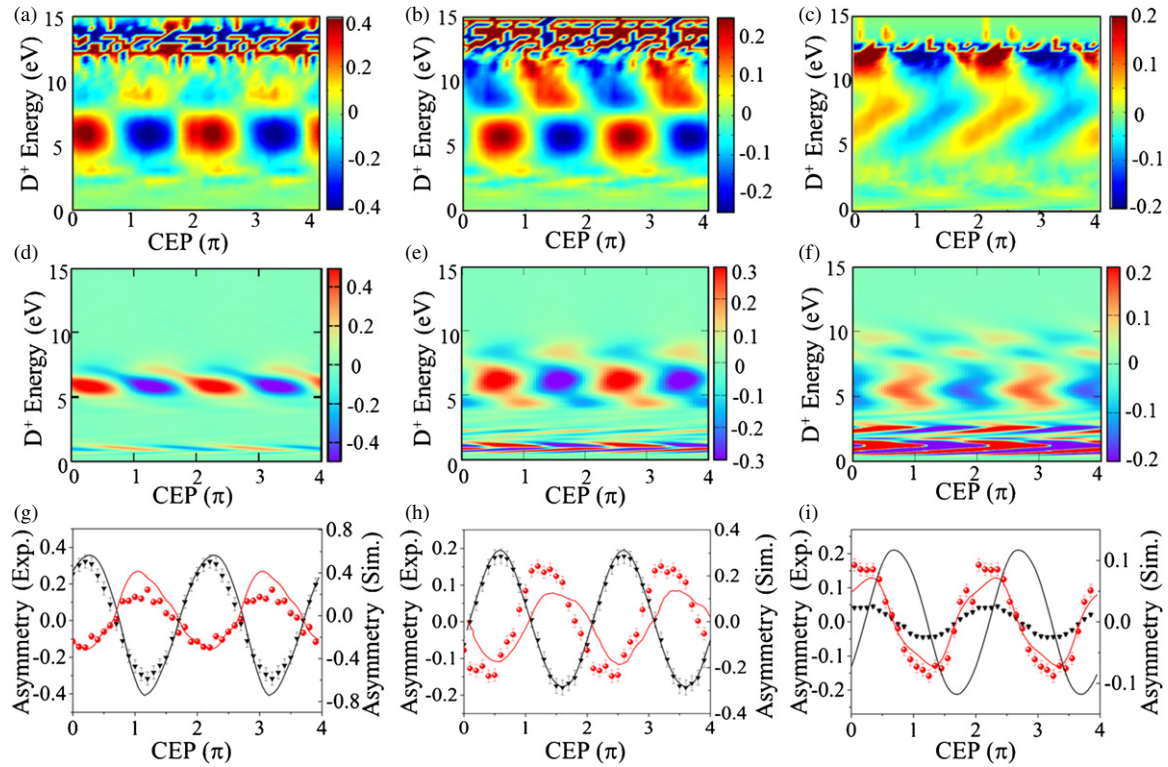
Figure 3. (a)–(c) Experimental asymmetry of the D^+ ion emission as a function of kinetic energy and CEP at intensities of (1.0 ± 0.3), (1.8 ± 0.3) and $(2.8 \pm 0.3) \times 10^{14}$ W cm^{-2}. (d)–(f) Simulated asymmetry maps of the D^+ ion emission for the experimental intensities. (g)–(i) Asymmetry oscillations obtained for integration over the regions of RCE-I (black triangles and lines for experiments and simulations, respectively) and RCE-II (red bullets and lines for experiments and simulations, respectively). The ranges for the RCE-I and RCE-II regions are given in table 1.

from autoionizing states of neutral molecular hydrogen which can also result in such high atomic ion kinetic energies [43]. The relevant Q3 and Q4 states, however, have long lifetimes which reduces their importance for electron localization [42].

4.2. CEP-dependence of the directional D^+ emission

The CEP- and energy dependence of the directional D^+ emission from the dissociative ionization of D_2 in the intense, near-single cycle laser pulses can be analysed with the experimental asymmetry parameter A_{ex} that is defined as

$$A_{ex}(\phi, E) = (Y_{up}(\phi, E) - Y_{down}(\phi, E))/$$
$$(Y_{up}(\phi, E) + Y_{down}(\phi, E)), \quad (8)$$

where $Y_{up/down}(\phi, E)$ are the yields within a certain angular range in the up/down directions along the polarization axis.

Figure 3 shows a comparison between the asymmetry maps A_{ex} from the experiments and A_{th} from the simulations. The experimental asymmetry is obtained by integrating the ion yield over an angular range of $\pm 45°$ around the laser polarization axis. The observed asymmetries for three selected intensities of $(1.0, 1.8$ and $2.8) \times 10^{14}$ W cm^{-2} oscillate with CEP within the entire range of detected D^+ energies and show relatively complex behaviour.

Experimental asymmetry contributions for the BS channel (below about 2 eV) are weak (less than ± 0.1) and they qualitatively agree with those reported by Kremer *et al* for 4.4×10^{14} W cm^{-2} at 760 nm [20]. Since BS requires

the cation to first stretch towards the crossing point for a one-photon transition from the ground to the excited $1\sigma_u$ state, BS can be suppressed with few-cycle pulses [56]. The fact that we still observe a very strong BS peak in the experiment with 4 fs pulses is likely due to the pedestal of the pulse, which can reach up to about 10% in intensity. The pedestal, due to its long effective pulse duration of about 25 fs, does not significantly contribute to the asymmetries and reduces asymmetry contributions from the 4 fs pulses. Larger asymmetries for BS have been reported for few-cycle pulses in the mid-infrared [22], where the pulse duration provides a better match to the timescale for BS.

In contrast to the asymmetry at low D^+ kinetic energies, for higher energies we obtained asymmetries of about ± 0.4 at an intensity of $(1.3 \pm 0.3) \times 10^{14}$ W cm^{-2}. The conditions of the experiment at this intensity are close to the study of Kling *et al* [17] using 5 fs pulses, where similar behaviour in this energy range was observed, only with smaller asymmetry amplitude (± 0.2). The difference in asymmetry amplitudes is assigned to the different pulse durations in both studies. The high energy part of the spectrum can be separated into different regions. The first one, which from here on is referred to as the RCE-I region, is centred around 6 eV up to 1.8×10^{14} W cm^{-2} and 7 eV at higher intensity. The present study also reveals a previously unobserved asymmetry contribution beyond the RCE-I region (from here on referred to as the RCE-II region), which exhibits a phase shift in its CEP-dependent oscillation of about π with respect to the
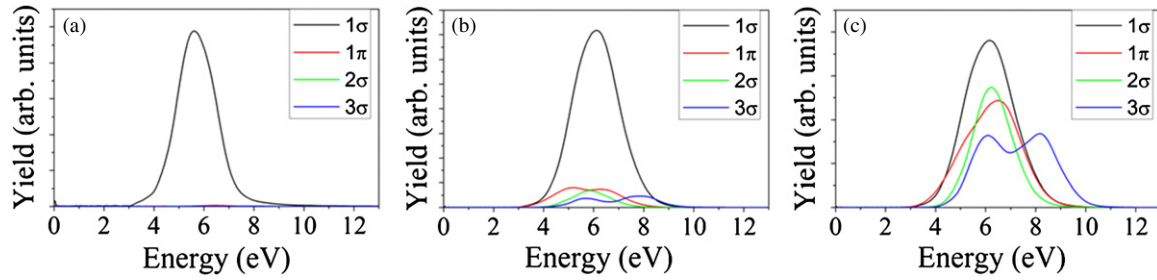
Figure 4. Simulated contributions from various D_2^+ states to the D^+ kinetic energy spectra for intensities of 1.0×10^{14} W cm^{-2} (a), 1.8×10^{14} W cm^{-2} (b) and 2.8×10^{14} W cm^{-2} (c). The data are volume and alignment angle averaged.

Table 1. Integration ranges for the RCE-I and RCE-II regions that were used to obtain the one-dimensional asymmetry data for experiments and simulations in figures 3(g)–(i).

		$I = 1.0 \times 10^{14}$ W cm^{-2}	$I = 1.8 \times 10^{14}$ W cm^{-2}	$I = 2.8 \times 10^{14}$ W cm^{-2}
RCE-I	Exp.	4–7.5 eV	3.7–7.3 eV	4–9 eV
	Sim.	5–6.5 eV	5–7 eV	4–7.5 eV
RCE-II	Exp.	8–9.5 eV	7.5–11.3 eV	9.5–11.8 eV
	Sim.	6.5–8 eV	7–10 eV	9–10 eV

RCE-I contribution at $(1.0 \pm 0.3) \times 10^{14}$ W cm^{-2}. This can be clearly seen from energy-integrated asymmetry plots for these two regions in figure 3(g). The simulations, as shown in figures 3(d) and (g), show the same pattern. The kinetic energy ranges for the RCE-I and RCE-II contributions are slightly lower in the simulations (potential reasons for the deviation were discussed in section 3.1). This has been taken into account in the integration ranges for the respective regions, which are listed in table 1.

With increasing intensity, the observed energy range for asymmetries increases and matches the range over which D^+ ions have been recorded for these conditions (see the kinetic energy spectra in figure 2(d)). In particular, the asymmetry contribution in the RCE-II region extends to about 12 eV already above $(1.8 \pm 0.3) \times 10^{14}$ W cm^{-2}. For the highest intensity in our study, the experimental RCE-II region is located in the range 9.5–11.8 eV, see figure 3(c) and table 1. The phase offsets of the asymmetry oscillations with CEP in the RCE-I and RCE-II regions are strongly dependent on the laser intensity as can be seen from figures 3(g)–(i).

At and above 1.8×10^{14} W cm^{-2}, the recollision energy is sufficient for the direct population of higher-lying excited states of D_2^+ at 730 nm. Therefore, although the additional contribution in the integrated D^+ spectra is still small, the asymmetry in the RCE-II region is assigned to dissociation from these higher-lying states, where laser-induced coupling of gerade and ungerade states after the population of these states creates the asymmetry.

Although the absolute CEP has not been precisely measured or assigned in our present study, the relative CEP shift between the measurements for different intensities can be analysed. The asymmetry oscillation near the spectral cutoff in the RCE-II region can serve as a reference. With respect to this reference, the asymmetry pattern for the RCE-I region shifts towards larger CEP values with increasing intensity. Furthermore, for intensities at and below 1.8×10^{14} W cm^{-2}, the asymmetry in this region does not show notable energy
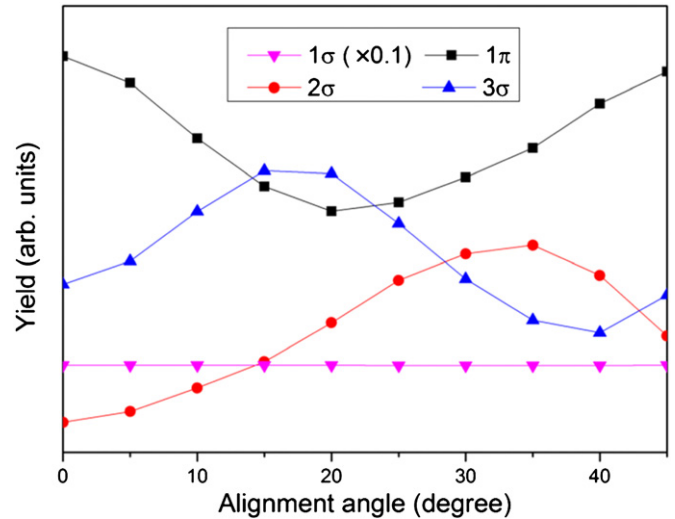

Figure 5. Simulated dissociation yields through different D_2^+ states as a function of molecular alignment with respect to the laser polarization axis for a laser intensity of 1.8×10^{14} W cm^{-2}.

dependence, in agreement with an earlier study [17] carried out at 1.2×10^{14} W cm^{-2}.

To understand the physics behind these observations, we analyse the simulation in detail by investigating the simulation results before volume and molecular alignment averaging. We find that (1) the lower energy D^+ peak below 8 eV mainly comes from 1σ, 2σ and 1π states while the high energy peak above 8 eV mainly comes from 3σ states (see figure 4); (2) the yield of 3σ increases as the alignment angle increases and reaches a maximum at about 15 degrees and decreases again as the alignment angle increases further, while the yield of 1π states changes oppositely (see figure 5). According to molecular tunnelling ionization theory [53], the tunnelling ionization rate weakly depends on the alignment, and the electron impact dissociation is isotropic if there is no influence of an external field. For the dissociation from a given specific
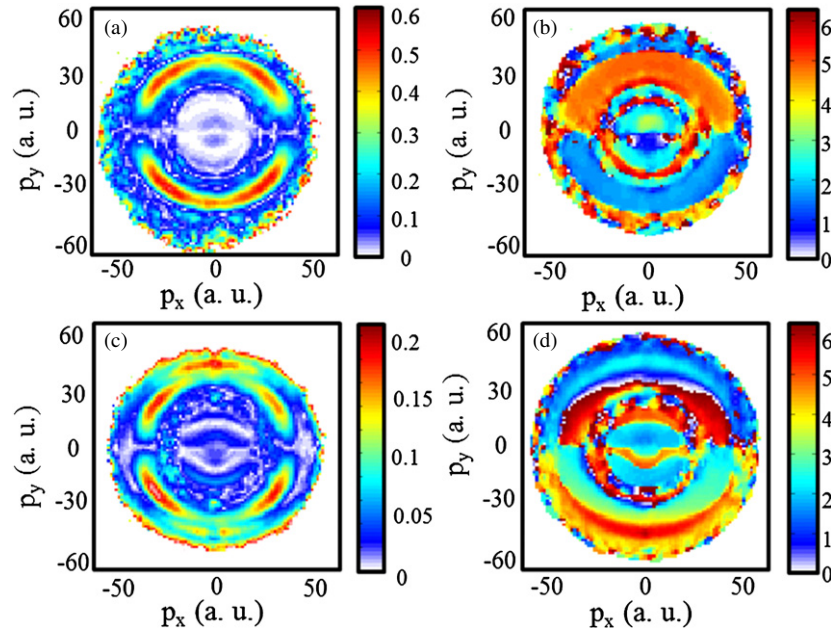
Figure 6. Momentum maps for the (a) amplitude and (b) phase offset (in rad) of the CEP-dependent part of the D^+ ion emission at a laser intensity of $(1.0 \pm 0.3) \times 10^{14}$ W cm^{-2}; (c) and (d) are the corresponding momentum maps for $(2.5 \pm 0.3) \times 10^{14}$ W cm^{-2}.
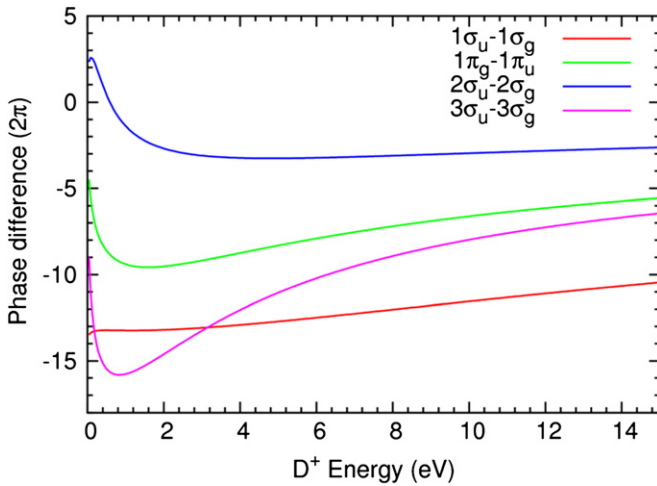

Figure 7. Phase differences between four groups of coupled excited states of D_2^+.

state the asymmetry parameters are always zero (conservation of parity). To obtain an asymmetry, an external field is needed to couple the gerade and ungerade parity states [57]. The total dissociation probability weakly depends on the CEP. Thus, when the 1π states (low D^+ kinetic energy) are excited to the 3σ states (high D^+ kinetic energy), the yield of D^+ ions from the 1π states is reduced while the one for dissociation via 3σ states is increased.

For low intensities below 1.8×10^{14} W cm^{-2}, the returning energy is not high enough to directly excite the D_2^+ ground state to 3σ states, and the 3σ states can only be populated by an additional laser-field-induced transition. The field-induced transition results in a dipole-like ring that is visible in the high energy part in figure 2(a). The phase offset in the CEP-dependent asymmetry oscillation between the two RCE regions can in this intensity range therefore be attributed to the field-induced transition from 1π to 3σ states.

As the intensity increases, a larger electron yield with a higher returning energy is obtained. The returning electron can now also directly excite the D_2^+ ground state to 3σ states. As compared to the field-induced transition process occurring for lower intensities, the 3σ states created by the recollision process should be in phase with other states. For high intensity the competition of the two processes, which are out-of-phase and in-phase, results in a complicated phase relationship between the asymmetries in the RCE-II region. Supporting this interpretation, in figure 2(c), the high energy contribution shows an isotropic (recollision-induced) and a dipole-like (field-induced transition) ring structure, which demonstrates the co-existence of the two mechanisms. When the intensity is increased further, the direct RCE of the 3σ states is gaining importance and the in-phase behaviour becomes dominant.

4.3. Angular distribution of the CEP-dependent D^+ emission

In addition to the analysis presented above, our phase-tagged VMI approach also permits investigation of the amplitude and phase of the CEP-dependent part of the ion emission as a function of p_x and p_y momenta. Here, for each position in momentum space, the CEP-dependent yield can be fitted with the following function [47, 58]:

$$A(p_x, p_y, \phi) = A_0(p_x, p_y) \cos[\phi + \Delta\phi(p_x, p_y)], \quad (9)$$

where p_x and p_y are the coordinates in momentum space, A_0 is the asymmetry amplitude and $\Delta\phi$ is the phase shift of the asymmetry oscillation with CEP. Note that ϕ is the phase measured by the phasemeter and has a constant offset to the absolute CEP. The momentum images are binned (within 2×2 pixels) in the fitting to improve the signal-to-noise ratio.

The amplitudes $A_0(p_x, p_y)$ and phase shifts $\Delta\phi(p_x, p_y)$ of the CEP-dependent D^+ ion emission are shown in figure 6 for laser intensities of 1.0, 2.5×10^{14} W cm^{-2}. The contributions with radial momenta around 12 au and 40 au
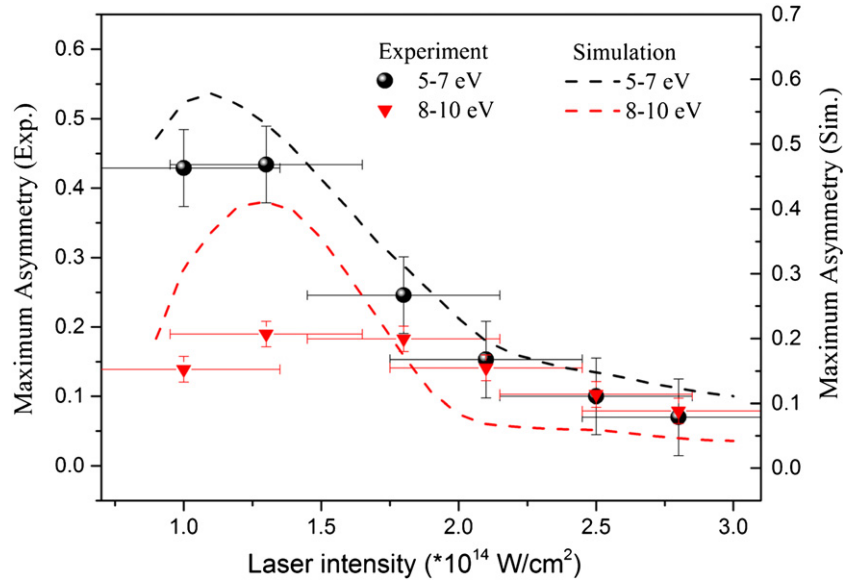
Figure 8. Amplitudes of the asymmetry oscillations for the two RCE regions as a function of the laser intensity obtained from experiments and simulations.

correspond to the BS and RCE regions. At an intensity of 1.0×10^{14} W cm^{-2} (figure 6(a)) no significant asymmetry is observed in the BS region (which we explained above by the role of the pedestal of the pulse). Only at higher intensities, starting at around 2.5×10^{14} W cm^{-2} (figure 6(c)) an asymmetry within an angular range of $\pm 60°$ is visible that is assigned to ATD. The RCE contribution to the asymmetry has a very wide angular distribution. A small depletion is observed along the polarization axis, which becomes strong at 2.5×10^{14} W cm^{-2} (figure 6(c)). The depletion goes along with the formation of an asymmetry contribution at slightly higher radial momenta with narrow angular distribution along the polarization axis. This contribution is assigned to the asymmetry being generated via a sequential process that involves RCE with subsequent laser-field-induced transition to the 3σ states. The dissociation energies of the 1σ, 2σ and 1π states are close to each other, so we cannot distinguish them in the kinetic energy spectra. From the alignment behaviour (figure 5) and the asymmetry amplitudes in figure 6(c), we may, however, conclude that the rings corresponding to the RCE-I region are mainly from dissociation via $1\pi_g$, while the outer rings in the RCE-II region are from dissociation via $3\sigma_u$ and $3\sigma_g$ states. The electron density of the $3\sigma_u$ state is narrowly distributed along the molecular axis.

Figures 6(b) and (d) show the phase offsets in the CEP-dependent asymmetry oscillations corresponding to figures 6(a) and (c), respectively. Phase offset changes between the RCE-I and RCE-II regions further support that different mechanisms are responsible for the population of the states. A more detailed analysis based on our simulations is given below.

4.4. Physical origin of the energy dependence of the directional ion emission

It is easy to understand that the asymmetry of the D$^+$ ion emission oscillates with CEP with a period of 2π, as shown

in figure 3. In order to understand the origin of the energy dependence of the asymmetry, we analyse the phases of the nuclear wave packets.

The asymptotic NWP in equation (2) can be written as

$$\chi_{i,g}(R, E) \rightarrow \exp[ikR + i\delta_{i,g}(E)] \tag{10}$$

and

$$\chi_{i,u}(R, E) \rightarrow \exp[ikR + i\delta_{i,u}(E)], \tag{11}$$

where $k = \sqrt{2\mu E}$, μ is the effective mass, $\delta_{i,g}(E)$ and $\delta_{i,g}(E)$ are the phase shifts for the gerade and ungerade states. Thus the electron localization to the up or down direction depends on the CEP as well as the difference between the paired phase shifts. Directions of D$^+$ ion emission are opposite to the electron localization direction. Figure 7 shows the phase difference between four groups of coupled states as a function of the dissociation energy. For the 1σ states, the phase changes by π per 2 eV near the energy range around 6 eV. For a high energy channel which originates from dissociation via 3σ states, the phase shift changes by π in the less than 1 eV energy range.

4.5. Amplitude of the CEP-dependent asymmetry as a function of intensity

Finally, we analyse the amplitude of the asymmetry oscillation as a function of the laser intensity for the RCE-I and RCE-II regions for both experimental data and simulations (see figure 8). The experimental results show the maximum asymmetry amplitude for both regions at around 1.3×10^{14} W cm^{-2}, with an amplitude of 0.43 and 0.24 for the RCE-I and RCE-II region, respectively. For higher laser intensities, the amplitudes for both channels decrease with increasing intensity. The simulation results show a similar trend. Furthermore, in the simulation the asymmetry for the RCE-I region is higher than for the RCE-II region, which is in qualitative agreement with the experimental results. The simulations predict slightly higher amplitudes for both RCE

J. Phys. B: At. Mol. Opt. Phys. **47** (2014) 124020

H Li *et al*

regions, but within the error bars of the experiments, hence, the agreement is very good.

The asymmetry of the dissociation mainly associates with the time at which the dissociative states are created in the laser field, or the initial time in equation (1). For lower intensity, some excited states can only be created when the returning energy is high enough (occurring within a narrow CEP range), which results in large asymmetry. For high intensities, the returning energy is high enough to create the excited states at almost any CEP. The yield of the excited states at different CEP depends on the energy of the returning electron [59]. When the returning energy is higher than the excitation energy (high intensity case), the yields of the excited states at different CEPs are almost identical so that the asymmetry vanishes. This explains the decrease of the asymmetry with increasing intensity.

Although the intensity dependence of the maximum asymmetry is in reasonable agreement between the experiment and the simulation, larger discrepancies still exist in the lower intensity region. In the present semi-classical simulations, the predicted maximum returning electron energy is 3.2 U_p, while the actual returning energy obtained from a quantum simulation is around 5–6 U_p [60, 61], much higher than the semi-classically predicted one. Here U_p is the ponderomotive potential and depends linearly on the laser intensity and is given as $U_p = I/(4\omega^2)$. Therefore, the present semi-classical simulation underestimates the return electron energy in the lower intensity region, and in turn underestimates the yield of the recollision-induced dissociation from higher excited states. In the simulation, the dissociation mainly comes from 1σ states at the lowest intensity. The asymmetry parameter is smaller due to the large energy gap between the two 1σ states (as shown in figure 1). This results in a stronger mismatch between the maximum asymmetry in experiments and simulations at the lower intensities.

5. Conclusions

We presented experimental and theoretical studies on the directional D^+ ion emission from the dissociative ionization of D_2 as a function of the laser intensity. A high-energy tail for the production of D^+ ions with kinetic energies above 8 eV is clearly identified in our studies and traced back to the dissociation from 3σ states of D_2^+ that are populated through electron recollision. The observed directional ion emission and angular distribution of emitted D^+ ions indicate that two mechanisms are responsible for the population of the 3σ states: (1) RCE with subsequent laser-field excitation dominating at low intensities (below 1.8×10^{14} W cm^{-2}) and (2) direct RCE at higher intensities. A decreasing asymmetry amplitude for the asymmetry in the ion emission from recollision-induced excitation is found which is explained on the basis of the variation of electron return energy with CEP. Our studies complement earlier work carried out at lower intensity. The observed mechanisms for the population of high-lying excited states of D_2^+ and phase offsets in the CEP-dependent asymmetries between the mechanisms are also relevant for such processes in other molecules.

References

[1] Schultze M *et al* 2010 *Science* **328** 1658
[2] Uiberacker M *et al* 2007 *Nature* **446** 627
[3] Kling M F, von den Hoff P, Znakovskaya I and de Vivie-Riedle R 2013 *Phys. Chem. Chem. Phys.* **15** 9448
[4] Krüger M, Schenk M and Hommelhoff P 2011 *Nature* **475** 78
[5] Zherebtsov S *et al* 2011 *Nature Phys.* **7** 656
[6] Cavalieri A L *et al* 2007 *Nature* **449** 1029
[7] Neppl S, Ernstorfer R, Bothschafter E M, Cavalieri A L, Menzel D, Barth J V, Krausz F, Kienberger R and Feulner P 2012 *Phys. Rev. Lett.* **109** 087401
[8] Schultze M *et al* 2013 *Nature* **493** 75
[9] Krausz F and Ivanov M 2009 *Rev. Mod. Phys.* **81** 163
[10] Johnson N G *et al* 2011 *Phys. Rev.* A **83** 013412
[11] Rathje T *et al* 2012 *J. Phys. B: At. Mol. Opt. Phys.* **45** 074003
[12] Wittmann T, Horvath B, Helml W, Schätzel M G, Gu X, Cavalieri A L, Paulus G G and Kienberger R 2009 *Nature Phys.* **5** 357
[13] Baltuska A *et al* 2003 *Nature* **421** 611
[14] Bergues B *et al* 2012 *Nature Commun.* **3** 813
[15] Zherebtsov S *et al* 2012 *New J. Phys.* **14** 075010
[16] Xie X *et al* 2012 *Phys. Rev. Lett.* **109** 243001
[17] Kling M F *et al* 2006 *Science* **312** 246
[18] Fischer B, Kremer M, Pfeifer T, Feuerstein B, Sharma V, Thumm U, Schröter C-D, Moshammer R and Ullrich J 2010 *Phys. Rev. Lett.* **105** 223001
[19] Kling M F, Siedschlag C, Znakovskaya I, Verhoef A J, Zherebtsov S, Krausz F, Lezius M and Vrakking M J J 2008 *Mol. Phys.* **106** 455
[20] Kremer M *et al* 2009 *Phys. Rev. Lett.* **103** 213003
[21] Xu H, Maclean J-P, Laban D E, Wallace W C, Kielpinski D, Sang R T and Litvinyuk I V 2013 *New J. Phys.* **15** 023034
[22] Znakovskaya I *et al* 2012 *Phys. Rev. Lett.* **108** 03002
[23] Ray D *et al* 2009 *Phys. Rev. Lett.* **103** 223201
[24] Wu J, Vredenborg A, Schmidt L P H, Jahnke T, Czasch A and Dörner R 2013 *Phys. Rev.* A **87** 023406
[25] Wu J *et al* 2013 *Nature Commun.* **4** 2177
[26] Singh K P *et al* 2010 *Phys. Rev. Lett.* **104** 023001
[27] Sansone G *et al* 2010 *Nature* **465** 763
[28] Rathje T, Sayler A M, Zeng S, Wustelt P, Figger H, Esry B D and Paulus G G 2013 *Phys. Rev. Lett.* **111** 093002
[29] Kling N G *et al* 2013 *Phys. Rev. Lett.* **111** 163004
[30] He F, Becker A and Thumm U 2009 *Phys. Rev. Lett.* **101** 213002
[31] Roudnev V and Esry B D 2007 *Phys. Rev.* A **76** 023403

J. Phys. B: At. Mol. Opt. Phys. 47 (2014) 124020

H Li *et al*

[32] Zhu J-Y, Liu B-K, Wang Y-Q, He H-X and Wang L 2010 *Chin. Phys. Lett.* **27** 093301

[33] Anis F and Esry B D 2012 *Phys. Rev. Lett.* **109** 133001

[34] Roudnev V, Esry B D and Ben-Itzhak I 2004 *Phys. Rev. Lett.* **93** 163601

[35] Tong X M and Lin C D 2007 *Phys. Rev. Lett.* **98** 123002

[36] Gräfe S and Ivanov M Y 2007 *Phys. Rev. Lett.* **99** 163603

[37] Kelkensberg F, Sansone G, Ivanov M Y and Vrakking M 2011 *Phys. Chem. Chem. Phys.* **13** 8647

[38] Lan P, Takahashi E J, Liu K, Fu Y and Midorikawa K 2013 *New J. Phys.* **15** 063023

[39] Bandrauk A D, Chelkowski S and Nguyen H S 2004 *Int. J. Quantum Chem.* **100** 834

[40] Martin F *et al* 2007 *Science* **315** 629

[41] Sanz-Vicario J L, Bachau H and Martin F 2006 *Phys. Rev. A* **73** 033410

[42] Fernandez J and Martin F 2001 *J. Phys. B: At. Mol. Opt. Phys.* **34** 4141

[43] Aoto T, Hikosaka Y, Hall R I, Ito K, Fernandez J and Martin F 2004 *Chem. Phys. Lett.* **389** 145

[44] Posthumus J H 2004 *Rep. Prog. Phys.* **67** 623

[45] Bucksbaum P H, Zavriyev A, Muller H G and Schumacher D W 1990 *Phys. Rev. Lett.* **64** 1883

[46] He H-X, Lu R-F, Zhang P-Y, Han K-L and He G-Z 2012 *J. Phys. B: At. Mol. Opt. Phys.* **45** 085103

[47] Süßmann F *et al* 2011 *Rev. Sci. Instrum.* **82** 093109

[48] Sayler A M, Rathje T, Müller W, Rühle K, Kienberger R and Paulus G G 2011 *Opt. Lett.* **36** 1

[49] Vrakking M J J 2001 *Rev. Sci. Instrum.* **72** 4084

[50] Tong X M, Zhao Z X and Lin C D 2003 *Phys. Rev. A* **68** 043412

[51] Tong X M, Ranitovic P, Hogle C W, Murnane M M, Kapteyn H C and Toshima N 2011 *Phys. Rev. A* **84** 013405

[52] Jin Y J, Tong X M and Toshima N 2010 *Phys. Rev. A* **81** 013408

[53] Tong X M, Zhao Z and Lin C D 2002 *Phys. Rev. A* **66** 033402

[54] Tong X M and Lin C D 2005 *J. Phys. B: At. Mol. Opt. Phys.* **38** 2593

[55] Alnaser A S *et al* 2004 *Phys. Rev. Lett.* **93** 183202

[56] McKenna J, Anis F, Sayler A M, Gaire B, Johnson N G, Parke E, Carnes K D, Esry B D and Ben-Itzhak I 2012 *Phys. Rev. A* **85** 023405

[57] Roudnev V and Esry B D 2007 *Phys. Rev. Lett.* **99** 220406

[58] Kling M F, Rauschenberger J, Verhoef A J, Hasovic E, Uphues T, Milosevic D B, Muller H G and Vrakking M J J 2008 *New. J. Phys.* **10** 025024

[59] Tong X M and Lin C D 2007 *J. Phys. B: At. Mol. Opt. Phys.* **40** 641

[60] Sasaki K, Tong X M and Toshima N 2009 *J. Phys. B: At. Mol. Opt. Phys.* **42** 165603

[61] Ishikawa T, Tong X M and Toshima N 2010 *Phys. Rev. A* **82** 033411